Impact of Non-Ideality on Stability and Performance in Benzaldehyde Production

G. Andriani,[a,*] G. Pio,[b] C. Vianello,[a] E. Salzano,[b] and P. Mocellin[a,c]

[a]Università degli Studi di Padova, Dipartimento di Ingegneria Industriale, Via Marzolo 9, 35131 Padova, Italia

[b]Università di Bologna, Dipartimento di Ingegneria Civile, Chimica, Ambientale e dei Materiali, Via Terracini 28, 40131 Bologna, Italia

[c]Università degli Studi di Padova, Dipartimento di Ingegneria Civile, Edile e Ambientale, Via Marzolo 9, 35131 Padova, Italia

doi: https://doi.org/10.15255/CABEQ.2025.2447

Original scientific paper
Received: September 23, 2025
Accepted: December 16, 2025

Exothermic reactive processes pose significant safety risks due to the possibility of thermal runaway. Reliable tools for the design, control, and optimization of such systems are therefore essential. Stability analysis provides a powerful framework, but its effectiveness depends on an adequate representation of reactor hydrodynamics. Following the pioneering work of Varma, Morbidelli, and Wu, tubular reactors have mainly been analyzed using ideal plug flow reactor (PFR) models, which may lead to a partial assessment of critical operating regimes. In particular, neglecting non-idealities such as axial dispersion can underestimate runaway risk and distort predicted stability limits.

In this work, the impact of non-ideal plug flow behavior on reactor performance and stability is investigated by comparing ideal and axially dispersed PFR models within a sensitivity-based stability analysis (VMWT). The methodology is applied to the design of a multitubular reactor for the liquid-phase oxidation of benzyl alcohol to benzaldehyde. The results show how incorporating axial dispersion yields a more realistic stability picture while preserving computational efficiency, thereby supporting safer and more robust reactor design.

Keywords
chemical reactors, stability and performance analysis, process safety, critical unit operations

Introduction

Developing robust and transparent approaches for chemical reactor design and the selection of optimal operating conditions is essential for advancing sustainable processes[1]. Achieving this goal requires a multidisciplinary strategy that balances market demands with the physical and chemical constraints of the system[2]. A major challenge lies in the limitations of existing models to accurately predict safety parameters. Reactor behavior must be described through the consistent integration of mass and energy balances, while also accounting for kinetics, thermodynamics, and transport phenomena[3].

For exothermic reactions, preventing runaway conditions is a primary concern, making operational safety and the avoidance of catastrophic incidents paramount during design and optimization[4].

Despite the critical importance of safety in reactor design, systematic frameworks for hazard evaluation remain limited. The Varma, Morbidelli, and Wu theory of parametric sensitivity analysis (VMWT) provides a robust foundation for assessing the safety of reactive systems[5,6]. Since its introduction, VMWT has been applied to a variety of reactor configurations, including batch reactors[7], continuous stirred tank reactors (CSTRs)[8] and packed bed reactors[9]. However, its application to plug flow reactors (PFRs) remains insufficiently explored, especially once non-idealities, such as axial dispersion, are considered. Although prior studies have addressed some aspects[10], a comprehensive evaluation using dimensionless parameters is still needed. Such an approach would improve the general applicability of the analysis and support the development of robust safety indices for integration into broader design frameworks, such as those emphasizing sustainability[11].

To illustrate the benefits of this refined methodology, this work considers the industrially relevant production of benzaldehyde as a case study. Benzaldehyde is a key intermediate used in the manufacture of perfumes, dyes, plasticizers, flame retardants, preservatives, pesticides, and pharmaceuticals[12,13], and serves as a flavoring agent and fragrance precursors[14]. The predominant industrial

*Corresponding author: giuseppe.andriani@unipd.it

route—catalytic oxidation of toluene with oxygen—suffers from limited selectivity, significant safety concerns, and environmental drawbacks[15–19]. Overoxidation readily leads to benzoic acid or CO_2 formation[20], requiring strict control of temperature, oxygen partial pressure, and catalyst properties[21]. Additional challenges include flammable mixtures, hot spots leading to thermal runaway[22], catalyst deactivation primarily due to coke deposition[23], and VOC emissions and waste streams management[24], all of which increase process complexity and cost[25].

These drawbacks motivate the exploration of alternative routes[26]. One promising option is the oxidation of benzyl alcohol with hydrogen peroxide in the presence of ammonium molybdate $(NH_4)_2MoO_4$ as a heterogeneous catalyst[27]. Despite being insoluble in both aqueous and organic phases, the catalyst can be efficiently recovered via sedimentation, mitigating fouling and extending operational lifetime. This pathway offers high selectivity, but safety remains a critical issue due to the possible violent decomposition of hydrogen peroxide and oxygen evolution[28]. Rigorous kinetic modeling and safety protocols are therefore necessary to ensure reliability and selectivity.

In addition to the above considerations, it is important to clarify why the present study focuses on conventional multitubular reactors. Although intensified technologies—such as microreactors[29], mesoscale devices[30,31], and advanced heat-exchange architectures[32,33] —have been widely investigated for the safe handling of highly exothermic reactions, their industrial penetration remains limited. Despite their superior heat and mass transfer performance, improved thermal control, and rapid dissipation of reaction heat, these technologies are still constrained by relatively low technology readiness levels (TRLs), scale-up challenges, and the small number of full-scale implementations[34,35]. Consequently, conventional multitubular flow reactors remain the standard configuration for industrial liquid-phase oxidations of this type.

In multitubular reactor analysis, the ideal PFR model is widely employed for preliminary safety screening, feasibility assessment, and sensitivity analysis. Its simplicity and compatibility with classical stability tools—particularly the VMWT—make it attractive for identifying critical regimes prior to developing detailed, equipment-specific models, even though no quantitative evidence confirms that the ideal PFR + VMWT combination provides the most reliable safety-oriented framework. In this work, sensitivity analyses are therefore compared for both ideal and axially dispersed PFRs, showing that the inclusion of axial dispersion introduces only a modest increase in complexity while yielding a more realistic yet computationally efficient model that avoids underestimating safety margins. Applying the VMWT to non-ideal PFRs allows evaluation of how flow deviations affect stability limits and quantification of the resulting shifts in operational boundaries—an essential step for constructing stability and performance diagrams and defining robust indices for sustainability-oriented design. The catalytic oxidation of benzyl alcohol to benzaldehyde with hydrogen peroxide is used as a case study, illustrating the practical relevance of the methodology for both process understanding and reactor design.

Methodology

This section begins by discussing the implementation of the VMWT for reactor safety evaluation (Section "Chemical reactor safety"). Subsequently, Sections "Plug flow reactor model" and "Case study: Benzaldehyde production" review the adopted models and the selected case study, respectively.

Chemical reactor safety

Designing and optimizing chemical reactors for exothermic reactions requires achieving high levels of safety and performance. Sensitivity analysis provides a powerful tool for assessing reactive systems by evaluating how the system's behavior responds to variations in design or operational parameters[36]. For runaway reaction prevention, the normalized sensitivity of the dimensionless temperature (Θ) with respect to the dimensionless heat of reaction (B) is often selected as the key observable[37]. This normalized sensitivity, denoted as S(Θ,B), quantitatively characterizes system behavior and is defined as in Eq. 1 [38].

$$S(\Theta;B)=\frac{B}{\Theta}\frac{\partial\Theta}{\partial B}=\frac{B}{\Theta}s(\Theta;B) \qquad (1)$$

When S(Θ,B) reaches its maximum value, the reactor transitions from a stable operational regime to a runaway condition[39]. Identifying the critical point where this bifurcation occurs is essential for preventing unsafe operation, and for fine-tuning system design and operating parameters to balance safety and productivity[40]. Determining the critical value of B, where this behavioral shift occurs, involves solving the constitutive governing equations of reactors in their dimensionless form[41]. These equations are coupled with an additional set of sensitivity equations, enabling precise identification of the bifurcation point.

The sensitivity equations are obtained by direct differentiation of the governing balance equations. For each i-th balance equation f_i associated with the

i-th dimensionless state variable y_i differentiation with respect to the parameter selected for the sensitivity analysis (here B) yields the general sensitivity equation reported in Equation 2:

$$\frac{\mathrm{d}s\left(y_i,B\right)}{\mathrm{d}z}=\frac{\mathrm{d}^2s\left(y_i,B\right)}{\mathrm{d}z^2}+\sum_{i=1}^{N_b}\frac{\partial f_i}{\partial y_i}\cdot s\left(y_i,B\right)+\frac{\partial f_i}{\partial B} \quad (2)$$

In Eq. 2, the second derivative with respect to the dimensionless reactor length, $\frac{\mathrm{d}^2s\left(y_i,B\right)}{\mathrm{d}z^2}$, is included. This term must be retained only for the axially dispersed PFR model, whereas it is omitted when the ideal PFR formulation (without axial dispersion) is adopted.

Plug flow reactor model

For the sake of completeness, the main aspects and differences between ideal PFR and non-ideal PFR with axial dispersion models will be presented in this section.

The ideal PFR model is a fundamental representation for tubular reactors, assuming ideal fluid dynamics under conditions of perfect turbulent flow[42]. In this model, only axial variations in system properties are considered. Each infinitesimal volume along the reactor axis is treated as perfectly segregated, with no exchange of mass, energy, or momentum between adjacent volumes. This idealized behavior is characterized by the Peclet number Pe→∞, indicating that convective transport dominates entirely. The dimensionless governing equations and boundary conditions for the ideal PFR model are well-established in the literature[6]. The governing equations used in this study are presented in Section "Case study: Benzaldehyde production".

For sensitivity analysis, these governing equations are differentiated with respect to B, using S(Θ,B) as the observable. This process yields the sensitivity equations and their corresponding boundary conditions, enabling a detailed evaluation of system stability.

The non-ideal PFR model with axial dispersion differs from the ideal PFR primarily due to a finite Pe number, reflecting imperfect axial segregation. This introduces back-mixing effects that must be accounted for in the analysis. In laminar flow, these effects are represented by molecular diffusivity and thermal conductivity, while in turbulent flow, they are characterized by turbulent mass and thermal dispersion coefficients, commonly referred to as material and thermal dispersion coefficients. The governing equations and their corresponding boundary conditions for the non-ideal PFR model are well-documented in the literature[43]. As with the ideal PFR, sensitivity equations and their boundary conditions are derived directly from the dimensionless governing equations, facilitating a systematic evaluation of reactor stability.

Case study: Benzaldehyde production

The design of a reactor for benzaldehyde (BzH) production is considered as a case study. BzH can be synthesized from benzyl alcohol (BnOH) in the presence of hydrogen peroxide (HP) and ammonium molybdate as a catalyst[27]. However, BzH is an intermediate oxygenated compound that requires careful reaction control to prevent further oxidation to benzoic acid (BzOH). At elevated temperatures, HP decomposes into oxygen and water[44]. The simultaneous presence of dissolved oxygen and BzH can accelerate its oxidation to BzOH, posing challenges for process stability and selectivity. Despite the importance of these reactions, kinetic data for the oxidation of BzH to BzOH in the liquid phase under the influence of dissolved oxygen are scarce in the literature. To address this gap, *ab initio* methods can be employed to model the reaction mechanism and provide a theoretical understanding of the underlying phenomena. One efficient approach is the use of the reaction mechanism generator (RMG), which avoids directly solving quantum mechanical equations while enabling the construction of detailed reaction models[45]. By integrating existing literature data on the conversion of BnOH to BzH (Reaction 1 – Eq. 3) and HP decomposition (Reaction 2 – Eq. 4), the subsequent oxidation of BzH to BzOH can be modelled (Reactions 3 and 4 – Eqs. 5 and 6). For clarity, Eqs. from 3 to 6 report both the chemical reactions considered in this study and their corresponding rate expressions. In Fig. 1 are reported the molecular structures of the considered organic compounds, as well as the reactions identifiers and kinetic data sources.

$$\mathrm{BnOH}+\mathrm{HP}\rightarrow\mathrm{BzH}+\mathrm{H_2O} \qquad \mathcal{R}_1=k_1C_{\mathrm{cat}}C_{\mathrm{BnOH}} \quad (3)$$

$$\mathrm{HP_{(l)}}\rightarrow\mathrm{H_2O_{(l)}}+0.5\ \mathrm{O_{2(g)}} \qquad \mathcal{R}_2=k_2C_{\mathrm{HP}} \quad (4)$$

$$\mathrm{BzH}+0.5\ \mathrm{O_{2(l)}}\rightarrow\mathrm{RAD} \qquad \mathcal{R}_3=k_3C_{\mathrm{BzH}}C_{\mathrm{O_2,liq}} \quad (5)$$

$$\mathrm{RAD}\rightarrow\mathrm{BzOH} \qquad \mathcal{R}_4=k_4C_{\mathrm{RAD}} \quad (6)$$

Essential thermodynamic parameters (i.e., heat capacities, densities, viscosities, surface tensions, and thermal conductivities) were obtained using established correlations from the literature[46–49]. The oxygen generated from the decomposition of hydrogen peroxide (HP) initially resides in the gas phase, and subsequently it transfers to the liquid phase, where its equilibrium concentration is determined using Henry's law. The associated mass transfer coefficients are calculated using well-documented correlations[50,51]. Heat transfer is equally pivotal, as it ensures process stability and optimal perfor-

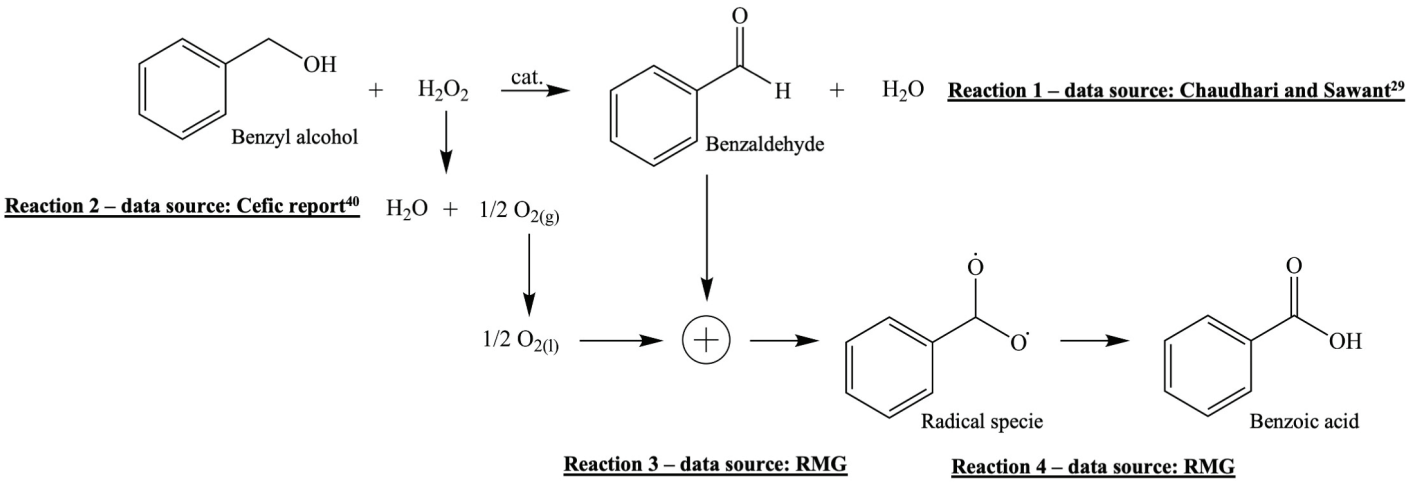

Fig. 1 – *Organic compound's molecular structure, reaction mechanism, and kinetic data sources*

mance. Depending on productivity and heat dissipation requirements, tubular reactors can be designed as single-tube or multi-tubular systems. Multi-tubular configurations, resembling shell-and-tube heat exchangers, are typically used for higher productivity, with the reactive medium flowing through a bundle of tubes surrounded by a cooling fluid on the shell side. Established references provide reliable correlations for these calculations[52]. Further considerations are required for calculating the turbulent Peclet number. For mass transport, the turbulent Peclet number is determined using the relationship $\mathrm{Pe}=\mathrm{Re}^{0.125}$, valid for liquid-phase $\mathrm{Re} > 2000$ [53]. For heat transport, axial heat dispersion is governed by the turbulent dispersion coefficient, which shares the same underlying mechanism as material dispersion. Consequently, the turbulent Peclet numbers for heat and mass transport are considered equivalent.

The complete set of governing equations is reported further in dimensionless form, consistent with the sensitivity analysis. Eq. (7) gives the general dimensionless mass balance, while Eqs. (8) and (9) describe the heat balances on the process and cooling sides, respectively. For all variables, $\mathrm{Pe}\to\infty$ recovers the classical ideal PFR formulation. Boundary conditions are specified at both ends of the reactor. At the inlet ($z=0$), Dankwerts conditions are applied (Eq. 10). At the outlet ($z=1$, Eq. 11), a negligible axial gradient is assumed, ensuring flux continuity. For the ideal PFR model, with infinite Peclet numbers, the inlet condition reduces to a simple specification of the feed values and no outlet condition is required.

$$\frac{\partial u_j}{\partial z}=\frac{1}{\mathrm{Pe}_{D_{z,j}}}\frac{\partial^2 u_j}{\partial z^2}\pm\xi\left(u_{j,L}^{eq}-u_{j,L}\right)+\mathrm{Da}\left(\nu_{j,1}R_1+\sum_{k=2}^{N_r}\nu_{j,k}R_k R_{r(k,1)}^{in}\right),\quad \forall j\in[1:N_c] \tag{7}$$

$$\frac{\partial\Theta}{\partial z}=\frac{1}{\mathrm{Pe}_{k_z}}\frac{\partial^2\Theta}{\partial z^2}-\mathrm{St}\left(\Theta-\Theta_{co}\right)+\mathrm{BDa}\left(R_1+\sum_{j=2}^{N_r}H_r(j,1)R_j R_{r(j,1)}^{in}\right) \tag{8}$$

$$\frac{\partial\Theta_{co}}{\partial z}=\frac{\xi\phi}{\mathrm{Pe}_{k_{z,co}}}\frac{\partial^2\Theta_{co}}{\partial z^2}+Y\mathrm{St}\left(\Theta-\Theta_{co}\right) \tag{9}$$

$$z=0\Rightarrow y_i=y_{i,\mathrm{in}}+\frac{1}{\mathrm{Pe}_{y_i}}\frac{\partial y_i}{\partial z},\quad \forall i\in[1:N_b] \tag{10}$$

$$z=1\Rightarrow\frac{\partial y_i}{\partial z}=0,\quad \forall i\in[1:N_b] \tag{11}$$

The reaction mechanism and kinetic model adopted in this study are summarized in Eqs. 3–6. The kinetic constants k_k for each k-th reaction are assumed to follow a generalized Arrhenius dependence. Table 1 reports the numerical parameters required to compute the reaction rates, and reaction enthalpies at 298 K.

Table 1 – *Quantities adopted in the kinetic model*

	m	k_∞	E_a	$\Delta\widetilde{H}_{r,298\,K}$
R1	0	$2.04\cdot10^7$ m^3 kmol^{-1} s^{-1}	84.7 kJ mol^{-1}	–19.26 kJ mol^{-1}
R2	0	$1.94\cdot10^6$ s^{-1}	86.1 kJ mol^{-1}	–98.03 kJ mol^{-1}
R3	0.695	$1.44\cdot10^4$ m^3 kmol^{-1} s^{-1} K^{-m3}	17.2 kJ mol^{-1}	–19.23 kJ mol^{-1}
R4	0.345	$5.15\cdot10^{10}$ s^{-1} K^{-m4}	29.3 kJ mol^{-1}	–378.40 kJ mol^{-1}

Table 2 – *Reference reactor configuration and operating conditions*

Quantity	Value	Quantity	Value
Inlet temperature [°C]	95	Number of tube pass [–]	2
Operating pressure [bar]	5	Number of shell pass [–]	2
Inlet flow rate – per tube [mol s^{-1}]	12	Number of tubes – per pass [–]	150
Inlet benzyl alcohol molar fraction [–]	0.13	Numbers of baffles - per pass [–]	20
Inlet hydrogen peroxide molar fraction [–]	0.13	Tubes internal diameter [mm]	50
Inlet water molar fraction [–]	0.71	Tubes width [mm]	5
Inlet catalyst molar fraction [–]	0.03	Tubes length – per pass [m]	6
Inlet cooling flow rate [kg s^{-1}]	25	Shell internal diameter [m]	1.10
Inlet cooling temperature [°C]	95		

Results and discussion

To better present the obtained results, this section includes specific sub-sections dedicated to the results obtained for the reactor design, trends in measurable parameters, and comparison of the employed models. More specifically, in Section "Reactor design", the reactor design outcomes are presented first. Subsequently, in Section "Performance analysis", the final temperature and conversion values for the same equipment configuration are compared under the assumptions of an ideal PFR and a PFR with axial dispersion. Finally, Section "Stability analysis" discusses the differences between these two modelling approaches, focusing on their impact on the system's stability.

Reactor design

This section details the proposed reactor configuration, considering only designs that achieve a minimum of 90 % conversion of benzyl alcohol (BnOH) as acceptable. Commercially available reactor tubes were selected, with lengths ranging from 1 m to 6 m and internal diameters of at least 1 inch, to eliminate the need for custom-made construction materials. Since the multi-tubular reactor configuration is analogous to a shell-and-tube heat exchanger, the design complies with TEMA standards.

A closer examination of the tube diameter highlights its impact on the validity of one-dimensional reactor models. In tubular reactors, increasing the diameter generally amplifies deviations from the assumptions of purely axial behavior, as radial temperature gradients may arise when heat is generated volumetrically in the fluid but removed only at the wall. Conversely, small tube diameters—such as the one used in this work—provide a higher external surface area per unit volume, enhancing heat removal relative to heat generation. The relevance of radial thermal gradients can be evaluated using the thermal Biot number, Bi. For $Bi<0.1$, radial conduction within the fluid is sufficiently fast compared with heat transfer at the wall, and the temperature profile can be considered radially uniform. In the present case, the calculated Biot number remains below this threshold along the entire tube, thereby justifying the use of a one-dimensional reactor model in the subsequent analysis.

Table 2 summarizes the parameters adopted for the reference configuration, while Fig. 2 illustrates a schematic representation of the proposed setup. The reactor design was initially developed using the ideal plug flow reactor (PFR) model. Axial dispersion effects were subsequently incorporated during the verification phase to assess the influence of back-mixing on reactor performance and to optimize the computational efficiency of the modeling approach.

Based on the parameters in Table 2, the inlet temperature was carefully selected to prevent the thermal decomposition of hydrogen peroxide (HP) in the feed mixture. Due to the thermal instability of

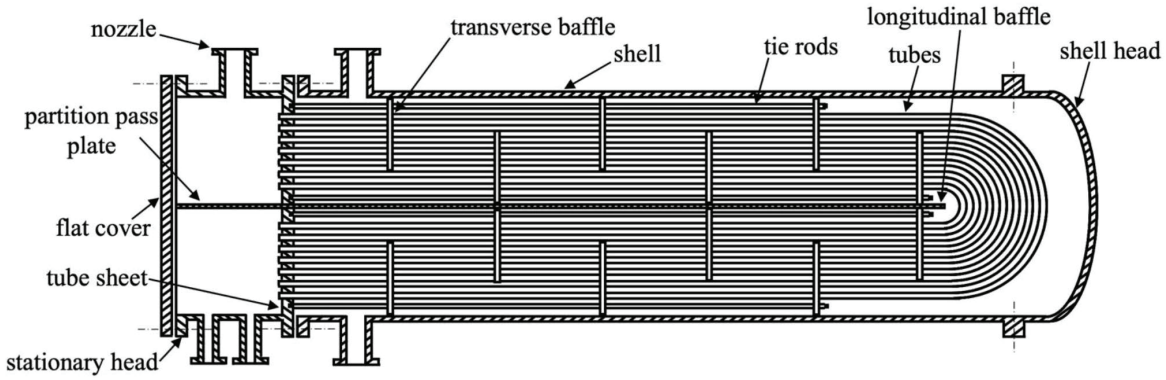

Fig. 2 – *Reactor configuration designed in this work for the conversion of benzyl alcohol to benzaldehyde*

HP and its associated safety risks, a 30 % w/w HP solution was chosen as an optimal compromise between safety and reactor performance. While a 50 % w/w HP solution would reduce the water content in the mixture, it would also significantly lower the maximum allowable operating temperature—from 100 °C to 80 °C. This reduced temperature would decrease the reaction rate, requiring an impractically long reactor or an excessive amount of catalyst, thereby offsetting any benefits from reduced water content and rendering the configuration unfeasible. To achieve the desired outlet conversion under the constraints outlined in Table 2, a total tube length of 12 m is required. This can be implemented using a single unit with tubes 6 m in length per pass, configured with two passes on both the tube side and the shell side. Given the exothermic nature of the reaction, co-current flow between the cooling fluid and the reactive mixture is recommended to optimize heat transfer efficiency[54]. A Type F shell configuration was selected for this purpose, ensuring consistent co-current flow of the cooling fluid relative to the reactive mixture. To further enhance operational efficiency and facilitate maintenance, a CFU configuration, as defined by TEMA standards, is recommended (Fig. 2). This design includes a shell separable from the tube sheet for maintenance, along with a flat cover on the head to allow easy access for internal tube-side cleaning. This configuration achieves a balance between safety, operational efficiency, and maintenance requirements.

Performance analysis

This section examines the outlet temperature and conversion values derived from the ideal and axial-dispersed PFR models. The reference inlet conditions and equipment configuration, as detailed in Section "Reactor design", serve as the basis for this analysis. For clarity and ease of interpretation, the results are presented in dimensional terms in Table 3.

Due to the relationship between dilution induced by the back-mixing and reduced reaction and thermal energy generation rates, the outlet temperature and conversion obtained using the axial-dispersed PFR model are lower than those predicted by the ideal model, as can be noted from Table 3. From a safety perspective, the maximum reached temperature is reduced. This factor enhances the thermal safety of the system. From a design perspective, the key issue is the achievable outlet values. Given fixed upstream and downstream process specifications, the reactor must be designed to meet the desired constraints. However, using an ideal model could result in an undersized system that may not be reliable. For example, the axial dispersion model predicts an outlet conversion lower than the 90 % target. If this occurs after the equipment has been installed, the operating parameters will need to be adjusted to meet process specifications. This highlights the importance of selecting the appropriate model, as incorrect assumptions may lead to discrepancies in operational performance.

Stability analysis

This section quantifies the impact of axial mixing on the overall stability and operational regime transitions of the equipment designed in Section "Reactor design". To achieve this, the results of the Varma, Morbidelli, and Wu Theory (VMWT) and sensitivity analysis are summarized in Table 4. The definitions and detailed explanations of the pseu-

Table 3 – *Ideal and axially-dispersed PFR models: comparison of estimated outlet conversion and temperature*

Ideal PFR model		Axially-dispersed PFR model	
Quantity	Value	Quantity	Value
Outlet temperature [°C]	113.8	Outlet temperature [°C]	112.5
Outlet BnOH conversion [%]	94.2	Outlet BnOH conversion [%]	86.4

Table 4 – *Transition boundaries between operating regimes*

Quantity	Ideal model	Axially-dispersed model
Operating B value [–]	2.00	2.00
Operating Da value [–]	0.53	0.53
Da value at the transition from PAO to HSO_1 regime	0.53	0.86
Da value at the transition from HSO_1 to HSO_2 regime	2.17	7.69
B value at the transition from stable to RUN regime	10.90	9.10

do-adiabatic (PAO), first hot spot (HSO_1), second hot spot (HSO_2), and runaway (RUN) operating region can be found in literature, together with the definitions of the dimensionless variables [6].

Analyzing the values presented in Table 4, the transition limit between the PAO and HSO_1 regions is considered first. In the ideal PFR model, no back-mixing occurs, resulting in the absence of reactant dilution and faster reaction progression compared to the axial-dispersed model. This leads to a quicker attainment of the temperature maximum. As a result, the ideal PFR predicts the PAO-HSO_1 transition at lower values of the Damköhler number (Da) while maintaining a constant value for B. This behavior is consistent with the theoretical expectation that the transition occurs when the temperature maximum is reached at the reactor outlet.

A similar trend is observed for the HSO_1-HSO_2 transition, where dilution and temperature suppression due to axial dispersion reduce the system's ability to achieve maximum yield. These findings reinforce the performance implications discussed in Section "Reactor design". Specifically, in the ideal PFR model, the reactor's operating point lies on the PAO-HSO_1 transition boundary (Table 3). In contrast, for the axial-dispersed model, the operating point shifts to within the PAO region due to the boundary displacement caused by back-mixing.

While these observations primarily influence reactor design and optimization, their safety implications are equally critical. Comparing the runaway region (RUN) boundaries reveals that transitioning from an ideal to an axial-dispersed reactor configuration results in an earlier onset of runaway behavior, occurring at lower values of B for a fixed Da. This highlights the importance of considering axial dispersion in the modeling approach to enhance the accuracy of performance predictions and ensure the reactor design remains both safe and reliable.

The selected operating point lies well within the PAO/HSO_1 region and remains far from the RUN boundary, indicating a high level of intrinsic safety for the proposed reactor configuration. This wide thermokinetic margin suggests that moderate disturbances—such as changes in feed composition, catalyst activity, or inlet temperature—are unlikely to shift the system toward conditions that could induce thermal runaway. The proposed multitubular configuration is therefore consistent with established industrial strategies for managing heat release in highly exothermic systems.

Although axial dispersion is known to influence stability limits, its systematic integration into the VMWT had not previously been reported for this class of liquid-phase oxidation systems. The results show that extending the VMWT to non-ideal flow conditions yields a more realistic and robust assessment of reactor stability, capturing subtle but significant effects of axial mixing on operational boundaries. This development is particularly relevant given the central role of the VMWT in evaluating runaway risk and supporting intrinsic-safety design.

From a practical standpoint, the dimensionless parameters obtained here enable the derivation of quantitative safety metrics. The critical B number provides a direct indicator of runaway onset, while distances in Da or B units between the PAO, HSO_1, HSO_2, and RUN regions quantify the stability margin of the nominal operating condition.

Conclusions

Runaway in exothermic processes remains a key challenge for the safe and reliable operation of industrial reactors. In this work, design principles were combined with a sensitivity-based stability analysis (VMWT) to support the development of safe and robust reactive systems, explicitly accounting for model uncertainty and non-ideal hydrodynamics. The methodology was applied to the industrial oxidation of benzyl alcohol to benzaldehyde, showing how stability theory and reactor design can be treated within a single, coherent framework.

The proposed equipment is a CFU TEMA multitubular reactor with two tube-side passes, a tube internal diameter of 2 inches, and 150 tubes per pass, designed to process an inlet flow rate of 1800 mol s^{-1}. A preliminary thermal analysis showed that the Biot number remained below 0.1 along the reactor length, indicating negligible radial temperature gradients and supporting the assumption of a radially uniform temperature field. This justifies the use of a one-dimensional model for this class of equipment. Within this framework, the inclusion of axial dispersion significantly affected the predicted behavior: compared with the ideal PFR, the dispersed PFR model revealed a wider runaway region and a

stronger sensitivity of temperature and conversion to back-mixing. These findings indicate that purely ideal models may underestimate thermal risk and lead to optimistic assessments of operability, whereas the axially dispersed model provides a more realistic and safety-oriented description.

Intensified reactor technologies (such as microreactors, mesoscale devices, and advanced heat-exchange designs) can provide better thermal control, but their industrial deployment is still limited by scale-up challenges and lower technology readiness. Conventional multitubular reactors therefore remain the most practical choice for large-scale liquid-phase oxidations such as the benzaldehyde process considered here. By extending the Varma–Morbidelli–Wu theory to axially dispersed PFRs, this study provides a more realistic yet still efficient stability framework and broadens the use of classical safety tools. The resulting stability and performance metrics indicate that the proposed operating point lies well within the safe region, confirming the robustness of the reactor configuration and the industrial relevance of the design approach.

Nomenclature

$B = \dfrac{\left(-\Delta\tilde{H}_{r1}\right)C_{\mathrm{BnOH},in}}{\rho\hat{C}_{p,mix}T_{in}}\gamma_1$ – Dimensionless heat of reaction

$\mathrm{Bi} = \dfrac{h_{int}D}{2k_{T,in}}$ – Biot number

BnOH – Benzyl alcohol

BzH – Benzaldehyde

BzOH – Benzoic acid

C – Dimensional concentration

$\hat{C}_p$ – Heat capacity per unit mass

co – Cooling side

CSTR – Continuous stirred tank reactor

D – Internal tube's diameter

$\mathfrak{D}_z$ – Turbulent mass axial dispersion coefficient

$\mathrm{Da} = \dfrac{\mathcal{R}_1\big|_{in}L}{v_z C_{\mathrm{BnOH},in}}$ – Damköhler number

E_a – Activation energy

eq – Equilibrium value

f – Fanning coefficient

f_i – *i*-th balance equation

h_{int} – Internal heat transfer coefficient

$H_r = \dfrac{\Delta\tilde{H}_{r(T)}}{\Delta\tilde{H}_{1(T)}}$ – Dimensionless heat of reaction ratio

HP – Hydrogen peroxide

HSO_1 – First hot-spot operation

HSO_2 – Second hot-spot operation

$k_k = k_{k\infty}T^{m_k}\exp\left(\dfrac{-E_{ak}}{R_gT}\right)$ – *k*-th kinetic constant

$k_{k\infty}$ – *k*-th kinetic constant pre-exponential factor

k_p – Kinetic unit factor

$k_{T,in}$ – Internal thermal conductivity

k_z – Turbulent heat axial dispersion coefficient

L – Liquid phase

L_p – Tube's length per pass

L_{tot} – Total reactor's length

m_k – *k*-th kinetic constant temperature exponent

mix – Mixture value

N_b – Total number of balance equations

N_c – Total number of components

N_r – Total number of reactions

n_T – Total number of tubes

P – Dimensional pressure

$\mathcal{P}$ – Dimensionless pressure

PAO – Pseudo-adiabatic operation

Pe – Peclet number

$\mathrm{Pe}_{\mathfrak{D}_{z,i}} = \dfrac{Lv_z}{\mathfrak{D}_{z,i}}$ – Turbulent mass axial Peclet number

$\mathrm{Pe}_{k_z} = \dfrac{\rho\hat{C}_{P,mix}Lv_z}{k_z}$ – Turbulent heat axial Peclet number

PFR – Plug flow reactor

Pr – Prandtl number

$R_k = \dfrac{\mathcal{R}_k}{\mathcal{R}_k\big|_{in}}$ – *k*-th dimensionless reaction rate

$\mathcal{R}_k$ – *k*-th dimensional reaction rate

RAD – Radical species

Re – Reynolds number

R_g – Universal gas constant

RMG – Reaction Mechanism Generator

$R^{in}_{r(k,1)} = \dfrac{\mathcal{R}_k\big|_{in}}{\mathcal{R}_1\big|_{in}}$ – *k*-th dimensionless reaction rate ratio

RUN – Runaway region

S(Θ;B) – Normalized sensitivity of Θ to the respect of B

s(Θ;B) – Local sensitivity of Θ to the respect of B

Sc – Schmidt number

$\mathrm{St} = \dfrac{4UL}{Dv_z\rho\hat{C}_{p,mix}}$ – Stanton number

T – Dimensional temperature

u – Dimensionless concentration

v_z – Superficial velocity

VMWT – Varma Morbidelli Wu theory

z – Dimensional axial coordinate

$\mathcal{Z} = \frac{z}{L_p}$ – Dimensionless axial coordinate

$\gamma_k = \frac{E_{ak}}{RT_{in}}$ – k-th dimensionless activation energy

$\Delta\widetilde{H}_r$ – Reaction enthalpy

$\theta = \frac{T - T_{in}}{T_{in}}\gamma_1$ – Dimensionless temperature

ν – Stoichiometric coefficient

Ξ – Dimensionless transport coefficient

ρ – Density

$\mathbf{Y} = \frac{\pi D^2 n_T v_z \rho \hat{C}_{p,mix}}{4\hat{C}_{p,co}\dot{m}_{co}}$ – Cooling side number

$\varphi = \frac{\rho \hat{C}_{p,mix} v_L}{\rho_{co}\hat{C}_{Pco} v_{L,co}}$ – Thermal capacities ratio

$\zeta = \frac{\mathrm{Pe}_{k_z}}{\mathrm{Pe}_{k_z,co}}$ – Thermal Peclet number ratio

References

1. *Andriani, G., Salano, L., Maria Bozzini, M., Mocellin, P., Manenti, F., Vianello, C.*, Sustainability-oriented process optimization for biogas to methanol: Balancing safety, economics, and environmental parameters, Ind. Eng. Chem. Res. **64** (2025) 14282. doi: https://doi.org/10.1021/acs.iecr.5c00494
2. *Andriani, G., Pio, G., Salzano, E., Vianello, C., Mocellin, P.*, Evaluating the thermal stability of chemicals and systems: A review, Can. Journ. of Chem. Eng. **103** (2024) 42. doi: https://doi.org/10.1002/cjce.25422
3. *Froment, G. F., Bischoff, K. B., De Wilde, J.*, Chemical Reactor Analysis and Design, John Wiley & Sons, Hoboken, 2011.
4. *Crowl, D. A., Louvar, J. F.*, Chemical Process Safety: Fundamentals with Applications, Pearson Education, Boston, 2011.
5. *Andriani, G., Mocellin, P., Pio, G., Vianello, C., Salzano, E.*, Enhancing safety in the storage of hazardous molecules: The case of hydroxylamine, J. Loss. Prev. Proc. Ind. **92** (2024) 105472. doi: https://doi.org/10.1016/j.jlp.2024.105472
6. *Varma, A., Morbidelli, M., Wu H.*, Parametric Sensitivity in Chemical Systems, Cambridge University Press, Cambridge, 1999.
7. *Morbidelli, M., Varma, A.*, A generalized criterion for parametric sensitivity: Application to thermal explosion theory, Chem. Eng. Sci. **43** (1988) 91. doi: https://doi.org/10.1016/0009-2509(88)87129-X
8. *Chemburkar, R. M., Morbidelli, M., Varma, A.*, Parametric sensitivity of a CSTR, Chem. Eng. Sci. **41** (1986) 1647. doi: https://doi.org/10.1016/0009-2509(86)85243-5
9. *Morbidelli, M., Varma, A.*, Parametric sensitivity and runaway in fixed-bed catalytic reactors, Chem. Eng. Sci. **41** (1986) 1063. doi: https://doi.org/10.1016/0009-2509(86)87193-7
10. *Copelli, S., Croci, S., Fumagalli, A., Derudi, M., Rota, R., Barozzi, M.*, Runaway problems in unsteady state tubular reactors, Chem. Eng. Trans. **53** (2016) 85. doi: https://doi.org/10.3303/CET1653015
11. *Zanobetti, F., Pio, G., Jafarzadeh, S., Muñoz Ortiz, M., Cozzani, V.*, Decarbonization of maritime transport: Sustainability assessment of alternative power systems, J. Clean. Prod. **417** (2023) 137989. doi: https://doi.org/10.1016/j.jclepro.2023.137989
12. Kirk-Othmer Encyclopedia of Chemical Technology, John Wiley and Sons, Hoboken, 2001.
13. *Zhou, W., Huang, K., Cao, M., Sun, F., He, M., Chen, Z.*, Selective oxidation of toluene to benzaldehyde in liquid phase over CoAl oxides prepared from hydrotalcite-like precursors, Reac. Kin. Mech. Cat. **115** (2015) 341. doi: https://doi.org/10.1007/s11144-015-0833-4
14. *Valentini, F., Ferracci, G., Galloni, P., Pomarico, G., Conte, V., Sabuzi, F.*, Sustainable highly selective toluene oxidation to benzaldehyde, Cat. MDPI **11** (2021) 262. doi: https://doi.org/10.3390/catal11020262
15. Ullmanns Encyclopedia of Industrial Chemistry, Wiley-VCH, Weinheim, 2011.
16. *Luo, H., Chen, W., Hu, J., Zhang, F., Hu, X.*, Highly selective oxidation of toluene to benzaldehyde in alkaline systems, Ind. Eng. Chem. Res. **62** (2023) 10051. doi: https://doi.org/10.1021/acs.iecr.3c01049
17. *Shoukat, H., Altaf, A. A., Hamayun, M., Ullah, S., Kausar, S., Hamza, M., Muhammad, S., Badshah, A., Rasool, N., Imran, M.*, Catalytic oxidation of toluene into benzaldehyde and benzyl alcohol using molybdenum-incorporated manganese oxide nanomaterials, ACS Omega **6** (2021) 19606. doi: https://doi.org/10.1021/acsomega.1c02163
18. *Guo, C. C., Liu, Q., Wang, X. T., Hu, H. Y.*, Selective liquid phase oxidation of toluene with air, Appl. Catal. A. Gen. **282** (2005) 55. doi: https://doi.org/10.1016/j.apcata.2004.11.045
19. *Wang, F., Xu, J., Li, X., Gao, J., Zhou, L., Ohnishi, R.*, Liquid phase oxidation of toluene to benzaldehyde with molecular oxygen over copper-based heterogeneous catalysts, Adv. Synth. Catal. **347** (2005) 1987. doi: https://doi.org/10.1002/adsc.200505107
20. *Lu, C., Hu, J., Meng, Y., Zhou, A., Zhang, F., Zhang, Z.*, The synergistic effect of benzyl benzoate on the selective oxidation of toluene to benzaldehyde, Chem. Eng. Res. Des. **141** (2019) 181. doi: https://doi.org/10.1016/j.cherd.2018.10.019
21. *Zhou, W., Huang, K., Cao, M., Sun, F., He, M., Chen, Z.*, Selective oxidation of toluene to benzaldehyde in liquid phase over CoAl oxides prepared from hydrotalcite-like precursors, Reac. Kin. Mech. Cat. **115** (2015) 341. doi: https://doi.org/10.1007/s11144-015-0833-4
22. *Stoessel, F.*, Thermal Safety of Chemical Processes, Wiley-VCH, Weinheim, 2020.
23. *Lapa, H. M., Martins, L. M. D. R. S.*, Toluene oxidation: CO_2 vs benzaldehyde: Current status and future perspective, Am. Chem. Soc. **9** (2024) 26780. doi: https://doi.org/10.1021/acsomega.4c01023
24. *Guo, C. C., Liu, Q., Wang, X. T., Hu, H. Y.*, Selective liquid phase oxidation of toluene with air, Appl. Cat. A. Gen. **282** (2005) 55. doi: https://doi.org/10.1016/j.apcata.2004.11.045
25. *Mal, D. D., Khilari, S., Pradhan, D.*, Efficient and selective oxidation of toluene to benzaldehyde on manganese tungstate nanobars: A noble metal-free approach, G. Chem. **20** (2018) 2279. doi: https://doi.org/10.1039/C8GC00123E

26. *Deng, C., Wang, K., Qian, X., Yao, J., Xue, N., Peng, L., Guo, X., Zhu, Y., Ding, W.*, Mild oxidation of toluene to benzaldehyde by air, Ind. Eng. Chem. Res. **62** (2023) 1688. doi: https://doi.org/10.1021/acs.iecr.2c03967
27. *Chaudhari, M. P., Sawant, S. B.*, Kinetics of heterogeneous oxidation of benzyl alcohol with hydrogen peroxide, Chem. Eng. J. **106** (2005) 111. doi: https://doi.org/10.1016/j.cej.2004.07.014
28. *Casson Moreno, V., Maschio, G.*, Screening analysis for hazard assessment of peroxides decomposition, Ind. Eng. Chem. Res. **51** (2012) 7526. doi: https://doi.org/10.1021/ie201690n
29. *Zhang, C., Zhang, J., Luo, G.,* Kinetics determination of fast exothermic reactions with infrared thermography in a microreactor, J. Flow. Chem. **10** (2020) 219. doi: https://doi.org/10.1007/s41981-019-00071-8
30. *Hoxha, J. L., Grogna, M., Calvo, S., Toye, D.,* Process intensification for zinc dithionite synthesis: Transition from batch to continuous mesofluidic reactor, Chem. Eng. J. **519** (2025) 164797. doi: https://doi.org/10.1016/j.cej.2025.164797
31. *Abdul Rahim, M. A., Phan, A. N., Harvey, A. P.,* Intensification of epoxidation of vegetable oils using a continuous mesoscale oscillatory baffled reactor, J. Adv. Man. Proc. **2** (2020) 1. doi: https://doi.org/ https://doi.org/10.1016/j.cej.2025.164797
32. *Zhang, J., Wang, K., Lin, X., Lu, Y., Luo, G.,* Intensification of fast exothermic reaction by gas agitation in a microchemical system, AIChE J. **60** (2014) 2724. doi: https://doi.org/10.1002/aic.14450
33. *Fratalocchi, L., Visconti, C. G., Groppi, G., Lietti, L., Tronconi, E.,* Intensifying heat transfer in Fischer-Tropsch tubular reactors through the adoption of conductive packed foams, Chem. Eng. J. **349** (2018) 829. doi: https://doi.org/10.1016/j.cej.2018.05.108
34. *Boffito, D. C.,* Scaling process intensification technologies: What does it take to deploy?, Chem. Eng. and Proc. – Proc. Int. **212** (2025) 110275. doi: https://doi.org/10.1016/j.cep.2025.110275
35. *Bugay, C. A., Caballas, M. C., Mercado, S. B., Rubio, J. F., Serote, P. K., Villarte, P. N., Vicente, R.,* A Review of Microreactors for Process Intensification, Eng. Proc. MDPI **67** (2024) 1. doi: https://doi.org/10.3390/engproc2024067021
36. *Zanÿr, M., Gavriilidis, A.*, An investigation of catalytic plate reactors by means of parametric sensitivity analysis, Chem. Eng. Sci. **57** (2002) 1653. doi: https://doi.org/10.1016/S0009-2509(02)00042-8
37. *Andriani, G., De Liso, B. A., Pio, G., Salzano, E.*, Design of sustainable reactor based on key performance indicators, Chem. Eng. Sci. **285** (2024) 119591. doi: https://doi.org/10.1016/j.ces.2023.119591
38. *Andriani, G., Mocellin, P., Pio, G., Salzano, E., Vianello, C.*, Design of storage equipment for unstable chemicals using sensitivity-based methods, Ind. Eng. Chem. Res. **64** (2025) 199529. doi: https://doi.org/10.1021/acs.iecr.5c00127
39. *Jiang, J., Jiang, J., Pan, Y., Wang, R., Tang, P.*, Investigation on thermal runaway in batch reactors by parametric sensitivity analysis, Chem. Eng. Technol. **34** (2011) 1521. doi: https://doi.org/10.1002/ceat.201000517
40. *Andriani, G., Pio, G., Vianello, C., Mocellin, P., Salzano, E.*, Safety parameters and stability diagram of hydroxylamine hydrochloride and sulphate, Chem. Eng. J. **482** (2024) 148894. doi: https://doi.org/10.1016/j.cej.2024.148894
41. *Zang, N., Qian, X. M., Shu, C. M., Wu, D.*, Parametric sensitivity analysis for thermal runaway in semi-batch reactors: Application to cyclohexanone peroxide reactions, J. Loss. Prev. Proc. Ind. **70** (2021) 104436. doi: https://doi.org/10.1016/j.jlp.2021.104436
42. *Salmi, T. O., Mikkola, J. P., Wärnå, J. P.*, Chemical Reaction Engineering and Reactor Technology, CRC Press, Boca Raton, 2018.
43. *Fogler, H. S.*, Elements of Chemical Reaction Engineering, Pearson, New Jersey, 2020.
44. Cefic Hydrogen Peroxide Technical Committee, Bulk storage guidelines, 2021.
45. *Pio, G., Dong, X., Salzano, E., Green, W. H.*, Automatically generated model for light alkene combustion, Comb. Flam. **241** (2022) 112080. doi: https://doi.org/10.1016/j.combustflame.2022.112080
46. *Green, D. W., Southard, M. Z.*, Perry's Chemical Engineers' Handbook, McGraw-Hill Education, New York, 2019.
47. *Akita, K., Yoshida, F.*, Bubble size, interfacial area, and liquid-phase mass transfer coefficient in bubble columns, Ind. Eng. Chem. Process Des. Develop **13** (1974) 84. doi: https://doi.org/10.1021/i260049a016
48. *Wu, G., Cao, E., Kuhn, S., Gavriilidis, A.*, A Novel approach for measuring gas solubility in liquids using a tube-in-tube membrane contactor, Chem. Eng. Tech. **40** (2017) 2346. doi: https://doi.org/10.1002/ceat.201700196
49. *Choong, K. S.*, Thermophysical properties of stainless steels, U.S. Energy Research and Development Administration, 1975.
50. *Demol, R., Vidal, D., Shu, S., Bertrand, F., Chaouki, J.*, Mass transfer in the homogeneous flow regime of a bubble column, Chem. Eng. Proc. Proc. Int. **144** (2019) 107647. doi: https://doi.org/10.1016/j.cep.2019.107647
51. *Calderbank, P. H., Moo-Young, M. B.*, The continuous phase heat and mass-transfer properties of dispersions, Chem. Eng. Sci. **16** (1961) 39. doi: https://doi.org/10.1016/0009-2509(96)81823-9
52. *Richardson, J. F., Harker, J. H., Backhurst, J. R.*, Coulson and Richardson's - Chemical Engineering, Elsevier, Oxford, 2020.
53. *Levenspiel, O.*, Chemical Reaction Engineering, John Wiley & Sons, New Jersey, 1999.
54. *Belfiore, L. A.*, Transport phenomena for chemical reactor design, John Wiley & Sons, New Jersey, 2003.